

RESEARCH

Open Access



The geometry of rest–spike bistability

Giuseppe Ilario Cirillo^{1*}  and Rodolphe Sepulchre¹

*Correspondence: gic27@cam.ac.uk
¹Department of Engineering,
University of Cambridge,
Trumpington Street, Cambridge, UK

Abstract

Morris–Lecar model is arguably the simplest dynamical model that retains both the slow–fast geometry of excitable phase portraits and the physiological interpretation of a conductance-based model. We augment this model with one slow inward current to capture the additional property of bistability between a resting state and a spiking limit cycle for a range of input current. The resulting dynamical system is a core structure for many dynamical phenomena such as slow spiking and bursting. We show how the proposed model combines physiological interpretation and mathematical tractability and we discuss the benefits of the proposed approach with respect to alternative models in the literature.

Keywords: Rest–spike bistability; Neuronal models; Slow–fast models

1 Introduction

Conductance-based models are by now well established as a fundamental modeling framework to connect the physiology and the dynamics of excitable cells. Ever since the seminal work of Hodgkin and Huxley [1], there has been a continuing effort in the literature to develop models that combine mathematical tractability and physiological interpretation. An interesting example is the two-dimensional model published by Morris and Lecar in 1981 [2]. Like Hodgkin–Huxley model, it captures the essential physiology of excitability: a spike results from the fast activation of an inward current followed by the slow activation of an outward current. The former provides positive feedback in the fast time-scale whereas the latter provides negative feedback in the slow time-scale. Because it is only two-dimensional, the model is also amenable to phase-portrait analysis without any reduction. Its geometry is similar to the one of FitzHugh–Nagumo model [3], the first mathematical model proposed to understand the core dynamics of the Hodgkin–Huxley model. In that sense, Morris–Lecar model combines the physiological interpretation of Hodgkin–Huxley model and the mathematical tractability of FitzHugh–Nagumo circuit.

In the present paper, we aim at capturing in a similar way the essence of rest–spike bistability, that is, the coexistence of a stable spiking attractor and a stable fixed point in a slow–fast model. The importance of this phenomenon is well acknowledged in the neurodynamics literature due to its role as a building block of neuronal patterns such as bursting [4, 5]. We obtain rest–spike bistability by adding one extra current in the Morris–Lecar model: an inward current with slow activation. The resulting model combines the three following features:

© The Author(s) 2020. This article is licensed under a Creative Commons Attribution 4.0 International License, which permits use, sharing, adaptation, distribution and reproduction in any medium or format, as long as you give appropriate credit to the original author(s) and the source, provide a link to the Creative Commons licence, and indicate if changes were made. The images or other third party material in this article are included in the article's Creative Commons licence, unless indicated otherwise in a credit line to the material. If material is not included in the article's Creative Commons licence and your intended use is not permitted by statutory regulation or exceeds the permitted use, you will need to obtain permission directly from the copyright holder. To view a copy of this licence, visit <http://creativecommons.org/licenses/by/4.0/>.

- (i) For a range of input currents, the model is rest–spike bistable, that is, a stable equilibrium coexists with a stable limit cycle. The geometry of the two attractors is robust to the time-scale separation in the sense that it persists in the limit of infinite time-scale separation.
- (ii) The model has the direct physiological interpretation of dynamics and attractors being shaped by three distinct currents (fast positive feedback (e.g. sodium activation), slow negative feedback (e.g. potassium activation), and slow positive feedback (e.g. calcium activation)).
- (iii) The model is amenable to a mathematical analysis by geometric singular perturbation theory.

We are not aware of other single-cell models in the literature combining those three features. Mathematical models of rest–spike bistability often lack the first feature above. For instance, a homoclinic bifurcation in the Morris–Lecar model only exists for a specific time-scale separation (see e.g. Table 3.1 in Sect. 3.2 of [4]). Limitations of such models with respect to the geometry of the attractors and the robustness of bursting are discussed in [6, 7]. We are only aware of two published models in which rest–spike bistability persists in the singular limit of infinite time-scale separation. The first one is the model proposed by Hindmarsh and Rose in 1982 [8] as a mathematical model aimed at capturing low-frequency spiking. The second one is the transcritical model proposed in 2011 as a two-dimensional reduction of a physiological model combining the currents of the Hodgkin–Huxley model with a slow inward (calcium) current [9]. Both models are planar and lack the second feature, that is, they can only be regarded as a mathematical reduction of a physiological conductance-based model.

This paper aims to contribute to the idea that balancing positive and negative feedback in the slow time scale is a key mechanism to generate rest–spike bistability. This viewpoint is at the core of the planar model in [6] and its importance from a physiological viewpoint is highlighted by [7]. Here we complement that work by studying how this mechanism can be naturally implemented in a physiological context: using two distinct slow currents, one providing negative feedback to restore the membrane potential, the other providing positive feedback to obtain two attractors separated by the stable manifold of a saddle.

The remainder of the paper is organized as follows. Section 2 presents the model and recalls the notions of geometric singular perturbation theory needed for its analysis. In Sect. 3 we study numerically the dynamics on the critical manifold, highlighting its persistence properties. Section 4 builds on this picture to derive conditions for multistability and monostability, we focus on the singular case and mention what hypotheses guarantee persistence. In Sect. 5 we discuss some variations of the same geometric picture, while in Sect. 6 we relate the Hindmarsh–Rose and the transcritical models to the one we are studying. We draw some conclusions in Sect. 7. Two appendices report additional details.

2 A model of rest–spike bistability

We consider a three-dimensional slow–fast conductance-based model defined by

$$\begin{aligned}
 \varepsilon \dot{v} &= i - i_{\text{ion}}(v, n, p), \\
 \dot{n} &= -n + S_n(v), \\
 \tau \dot{p} &= -p + S_p(v),
 \end{aligned}
 \tag{1}$$

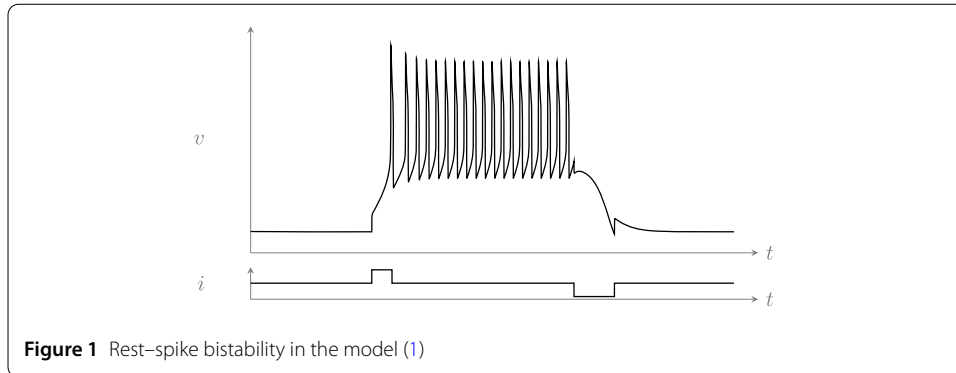


Figure 1 Rest-spike bistability in the model (1)

where ε is a small parameter. The total ionic current is the sum of a leak current and three voltage-gated currents:

$$\begin{aligned}
 i_{\text{ion}} &= g_l(v - v_l) + S_m(v)(v - 1) + n(v + 1) + p(v - 1) \\
 &= c(v) + n(v + 1) + p(v - 1).
 \end{aligned}
 \tag{2}$$

The parameters $-1 < v_l < +1$ that appear in the equation can be thought of as reversal potentials. In the absence of an external current i , the voltage range $[-1, 1]$ is positively invariant. The currents $S_m(v)(v - 1)$ and $p(v - 1)$ are then negative (*inward* currents) whereas the current $n(v + 1)$ is positive (*outward* current). The variables n and p are gating (positive) variables that model the slow activation of the inward current $p(v - 1)$ and of the outward current $n(v + 1)$. The inward current $S_m(v)(v - 1)$ has *instantaneous* activation, a standard simplification for currents that activate in the fast time-scale. The functions $S_x(v)$ correspond to activation functions that we assume of the form

$$S_x = \frac{g_x}{2} \left(\tanh\left(\frac{v - a_x}{b_x}\right) + 1 \right).
 \tag{3}$$

Here the multiplicative factor g_x corresponds to the maximal conductance associated to the current x . We find it convenient to write the equations in this form, rather than including maximal conductances in the voltage equation, because this allows us to change maximal conductances of slow currents without modifying the critical manifold of the system. A consequence of this is that the dynamics of p and n lies between zero and the corresponding maximal conductance, i.e. $p \in [0, g_p]$ and $n \in [0, g_n]$.

The key property of the model is the presence of the slow inward current $p(v - 1)$. In the absence of this current, the model is two-dimensional and has a phase portrait similar to the classical FitzHugh–Nagumo model. With this additional slow inward current, both continuous spiking and rest coexist for the same value of applied current, as shown by the simulation in Fig. 1 (see Appendix B for numerical values of the parameters).

We note that similar phenomena can be obtained with a current of the type $p(v + 1)$ where p inactivates, i.e. decreases as v increases. Physiologically this corresponds to an outward current that inactivates slowly, rather than an inward current that activates slowly. Both types of currents model a source of positive feedback in the slow time-scale [10]. A classical example of slowly inactivating outward current is the *A*-type potassium current [11].

We use geometric singular perturbation theory [12] to study the slow–fast system (1) as ε tends to zero. The singular limit of this model is the differential-algebraic system

$$\begin{aligned} 0 &= i - i_{\text{ion}}(v, n, p), \\ \dot{n} &= -n + S_n(v), \\ \tau \dot{p} &= -p + S_p(v), \end{aligned} \tag{4}$$

which we call slow dynamics or reduced system. After rescaling time, the same limit leads to the layer dynamics

$$\begin{aligned} v' &= i - i_{\text{ion}}(v, n, p), \\ n' &= 0, \\ p' &= 0, \end{aligned} \tag{5}$$

where $'$ refers to differentiation with respect to the fast time $\tau = t/\varepsilon$.

The reduced system (4) is constrained to the critical manifold C_0 , defined by

$$i_{\text{ion}}(v, n, p) = i \tag{6}$$

and corresponding to fixed points of the layer dynamics (5). Normally-hyperbolic compact subsets of C_0 persist as invariant manifolds of (1) for ε small enough. These manifolds are not necessarily unique, but we assume one family of perturbation C_ε has been fixed and call them slow manifolds.

Perturbations of subsets of C_0 maintain their type of stability with corresponding (local) stable and unstable manifolds. These admit invariant foliations, with each point on the critical manifold acting as base for a fiber. Invariance of the foliation can be interpreted as points on each fiber “shadowing” the corresponding base point, in forward time for the stable manifold and backward for the unstable. Points on C_ε follow a dynamics that is a regular perturbation of the reduced system (4); in the following we refer to this perturbation as slow dynamics.

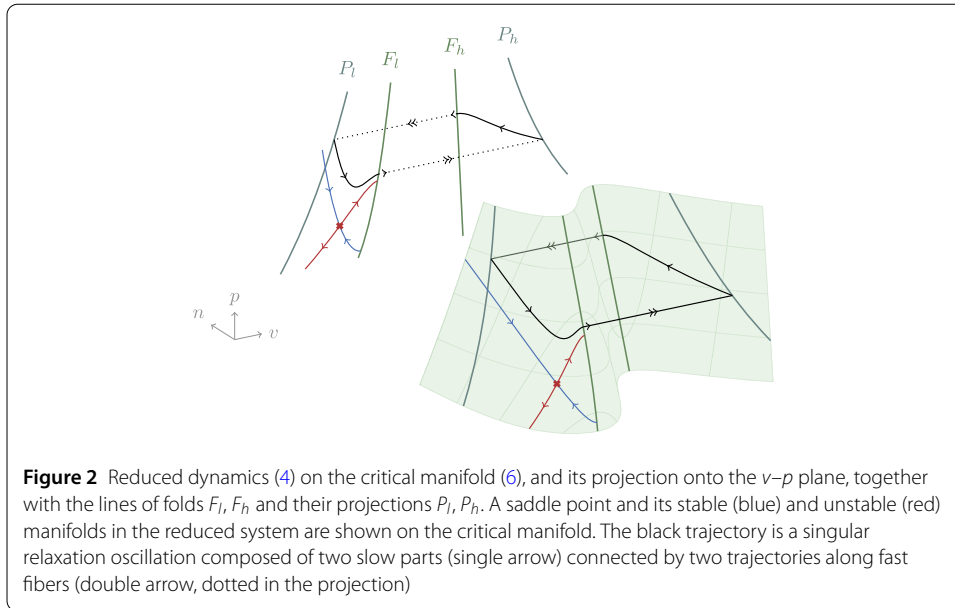
A point x on the critical manifold is normally hyperbolic if it is a hyperbolic fixed point of the layer dynamics (5). If this is the case, as $\varepsilon \rightarrow 0$ the fibers based at x tend to its stable and unstable manifolds in the layer dynamics (5). For (1) the layer dynamics is one dimensional, so that hyperbolic fixed points are either attractive or repulsive, with their invariant manifolds corresponding to lines with n and p constant.

We consider parameter ranges for which the critical manifold can be divided in three normally-hyperbolic branches. These are separated by two lines of folds that we call F_l and F_h , and verify

$$\frac{\partial i_{\text{ion}}}{\partial v} = \frac{dc}{dv}(v) + n + p = 0. \tag{7}$$

The two lines of folds are connected by an unstable branch M . The other branches, S_l and S_h , are both stable. Figure 2 shows the typical shape of the critical manifold for fixed i .

Around any point away from the lines of folds, the critical manifold admits a parametrization in the slow variables n and p . However, this local parametrization cannot be



made global due to the presence of folds. Following [13–15], we use v and p to obtain a parametrization valid in the interval $v \in (-1, 1)$. This is achieved by solving (6) for $n(v, p, i)$. The corresponding projection is shown in Fig. 2.

The reduced dynamics in these coordinates is obtained differentiating (6):

$$\begin{aligned} \frac{\partial i_{\text{ion}}}{\partial v} \dot{v} &= -\frac{\partial i_{\text{ion}}}{\partial n} \dot{n} - \frac{\partial i_{\text{ion}}}{\partial p} \dot{p}, \\ \tau \dot{p} &= -p + S_p(v). \end{aligned} \tag{8}$$

The first equation becomes singular on the lines of folds $\frac{\partial i_{\text{ion}}}{\partial v} = 0$. Multiplication by $\frac{\partial i_{\text{ion}}}{\partial v}$ recovers a regular differential equation:

$$\begin{aligned} \dot{v} &= -\frac{\partial i_{\text{ion}}}{\partial n} \dot{n} - \frac{\partial i_{\text{ion}}}{\partial p} \dot{p}, \\ \tau \dot{p} &= \frac{\partial i_{\text{ion}}}{\partial v} (-p + S_p(v)). \end{aligned} \tag{9}$$

The two systems (8) and (9) share the same trajectories with different time parametrizations. Moreover, in (9) time is reversed on the unstable branch $\frac{\partial i_{\text{ion}}}{\partial v} < 0$ and new fixed points can appear on the lines of folds. These verify

$$\frac{\partial i_{\text{ion}}}{\partial v} = 0, \quad \frac{\partial i_{\text{ion}}}{\partial n} \dot{n} + \frac{\partial i_{\text{ion}}}{\partial p} \dot{p} = 0. \tag{10}$$

They are called folded singularities [13].

Away from the lines of folds the two systems (8) and (9) are largely equivalent, but important differences occur in the neighborhood of F_l and F_h . Moreover, near these lines the perturbed dynamics is no longer constrained by normal hyperbolicity, in particular it cannot be obtained as a regular perturbation of the reduced system (8). Different phenomena are possible. The least degenerate situation occurs when the desingularized vector field is

never zero along these lines:

$$\frac{\partial i_{\text{ion}}}{\partial n} \dot{n} + \frac{\partial i_{\text{ion}}}{\partial p} \dot{p} \neq 0. \tag{11}$$

Under this assumption the desingularized vector field (9) can point either to the unstable branch or the stable one. Assuming the additional nondegeneracy condition

$$\frac{\partial^2 i_{\text{ion}}}{\partial v^2} \neq 0, \tag{12}$$

the first case corresponds to jump points, at which the reduced system (8) admits two solutions backwards in time but none in forward time. For $\varepsilon > 0$ a stable branch of C_ε near these points can be continued using the flow [14]. Doing so shows that trajectories on the slow manifold pass the folds and reach a fiber contained in the stable manifold of the other stable branch of C_ε , with the flow contracting the direction transverse to the manifold.

Condition (11) corresponds to the vector field being transverse to the critical manifold, a condition which is violated at folded singularities. These are fixed points of the desingularized system (9), but not necessarily fixed points of the reduced dynamics (8). As a consequence, they can be reached in finite time. Depending on the type of fixed point they can correspond to the singular limit of canard trajectories, i.e. intersections between stable and unstable branches of the slow manifold [13]. Generically, the desingularized flow changes direction at these points. Hence, a folded singularity delimits the set of jump points on a line of folds [15].

3 Reduced dynamics

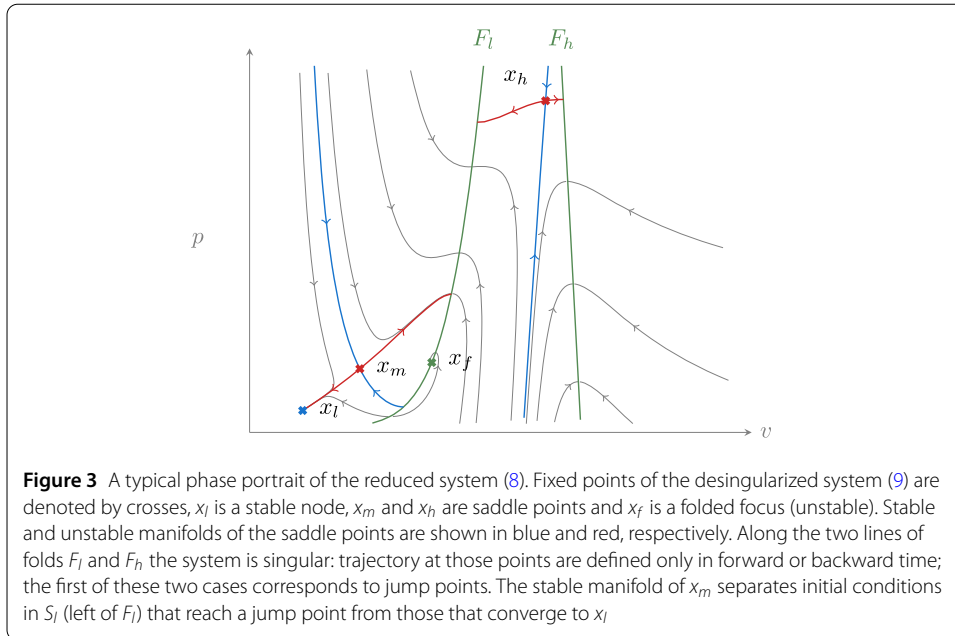
We will now study the reduced system (8), often with the aid of its desingularized version (9). Fixed points can be parametrized by v through the steady-state $i-v$ curve

$$i_s(v) := i_{\text{ion}}(v, S_n(v), S_p(v)). \tag{13}$$

This is shown in Fig. 6 and is an S-shaped curve, with two folds separating three families of fixed points $\mathcal{X}_l, \mathcal{X}_m$ and \mathcal{X}_h ; \mathcal{X}_l corresponds to low voltages, \mathcal{X}_m to intermediate voltages and \mathcal{X}_h to high voltages. For fixed i , we denote points in each family with corresponding lower-case letters x_l, x_m and x_h . In addition to these three fixed points, the desingularized dynamics (9) has a folded singularity $x_f \in F_l$. For parameter values reported in Appendix B, and i in the range of interest in this section, this point is a focus and does not lead to canard trajectories [13]; it only delimits jump points on F_l .

Figure 3 shows the typical phase portrait of the reduced system (8). The fixed point x_l is a stable node, while x_m and x_h are both saddle points. Their stable and unstable manifolds do not extend beyond F_l and F_h due to loss of existence and uniqueness along these lines. In particular, unstable manifolds terminate at jump points.

For $\varepsilon > 0$ hyperbolic fixed points persist in the slow dynamics with their stable and unstable manifolds [12, 16]. In the perturbed system (1) these fixed points are still hyperbolic. In particular, saddle points remain saddle, with their invariant manifolds being obtained as a combination of trajectories in the slow dynamics and fast fibers. The unstable manifold of x_m is completely contained in the slow manifold. Its stable manifold, instead, is two



dimensional; it includes the stable manifold in C_ε and all fast fibers based on that curve. In the singular limit this surface tends to the stable manifold of x_m in the reduced system (8) and all nearby segment with constant n and p that intersect it. Similarly, x_h perturbs to a saddle with a one-dimensional stable manifold and a two-dimensional unstable manifold.

Adding a trivial equation for i to (1), the same is true for the family of fixed points $x_m(i)$. At least for i in a small interval, this family persists together with its two-dimensional unstable manifold and three-dimensional stable one. Sections of these manifolds for fixed i coincide with the invariant manifolds of the corresponding fixed point.

When i varies on larger domains, the outlined phase portrait can undergo two distinct qualitative changes: increasing i leads to a fold of the $i-v$ curve at which x_l and x_m merge in a saddle-node bifurcation, leaving only one fixed point $x_h \in M$. Likewise, decreasing i , x_m and x_h reach a similar fate, leaving $x_l \in S_l$ as the only fixed point.

To obtain this second bifurcation it is necessary that one of the two fixed points crosses the line F_l and changes branch.⁴ In our case x_m crosses F_l . This passage corresponds to an exchange of stability with the folded singularity through a folded saddle-node [17]. Beyond this crossing, the folded singularity is a saddle, while x_m is a node of the reduced system. In a similar fashion increasing the applied current leads to x_h crossing F_h , which happens once x_h is the only fixed point left. After this crossing, x_h is a stable fixed point on an attractive branch.

Finally, varying i can lead to changes in the type of folded singularity. As already mentioned $x_m \in F_l$ corresponds to a folded saddle-node, thus varying i and moving x_m between branches leads to different types of folded singularity: it is a saddle when $x_m \in M$ and a node when $x_m \in S_l$. Both situations lead to canard trajectories [13]. Moreover, since x_f is a focus in the phase portrait described above, it has to change to a node before becoming a folded saddle-node.

4 Rest–spike bistability

Returning to the phase portrait in Fig. 3, we now analyze the global return mechanism that leads to rest–spike bistability.

In the singular limit $\varepsilon = 0$, trajectories on stable branches of the critical manifold \mathcal{C}_0 stay on it until they reach a line of fold in correspondence of a jump point. Once one of these points is reached the singular trajectory is continued along a fast fiber with constant n and p , reaching the opposite branch as shown in Fig. 2. The points at which these singular trajectories arrive correspond to the projections of F_l and F_h along fast fibers. We call these projections $P_l \subset S_l$ and $P_h \subset S_h$.

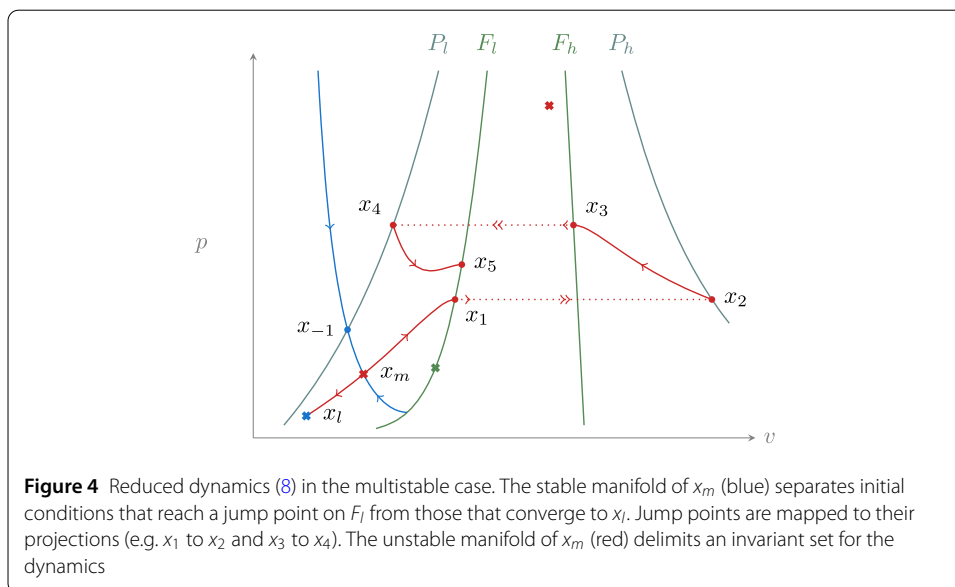
Based on this property, we can analyze the singular system referring only to the v – p plane and the reduced dynamics: when a trajectory reaches a jump point it is transported to the corresponding projection keeping p fixed, as shown in Fig. 2 for a limit cycle.

Rest–spike bistability follows from how the stable and unstable manifold of x_m constrain trajectories. The role of the stable manifold is simple, it separates initial conditions on S_l that reach a jump point on F_l from those that remain on the critical manifold and tend to x_l . The unstable manifold, instead, determines if the system is multistable. This is the case if the unstable manifold stays away from x_l . Otherwise almost all trajectories converge to x_l . We treat these two situations separately in the next sections.

4.1 Bistability

In the following we denote by x_1 the intersection of the unstable manifold of x_m with F_l , and by x_{-1} the intersection of the stable manifold of x_m with P_l . Following the singular flow from x_1 leads to $x_2 \in P_h$, then to $x_3 \in F_h$ and back to P_l at x_4 (see Fig. 4). We recall that given the dynamics (1) we can assume that p lies in the interval $[0, g_p]$, where g_p is the maximal conductance appearing in (3).

Assume that the trajectory starting at x_4 reaches a jump point on F_l (x_5), as shown in Fig. 4. Consider the segment $I_l \subset P_l$ between x_4 and $p = g_p$. The reduced dynamics maps this segment to F_l in finite time, defining a map $\Pi_l : I_l \rightarrow F_l$. Clearly the same map can be defined using the desingularized reduced system (9), thus as long as this vector field is



transverse to F_l at all points in $\Pi_l(I_l)$ the map is smooth. We note that this is equivalent to $\Pi_l(I_l)$ not containing folded singularities. Similarly, on S_h we define the segment $I_h \subset P_h$ between x_2 and $p = g_p$, and a corresponding map $\Pi_h : I_h \rightarrow F_h$. We denote the projection along fast fibers by Π_f (from F_l to P_h and from F_h to P_l). Since the dynamics is bounded by the line $p = g_p$, by construction we have

$$\Pi_f \circ \Pi_l(I_l) \subset I_h, \quad \Pi_f \circ \Pi_h(I_h) \subset I_l, \tag{14}$$

which allows us to define the singular Poincaré map

$$\Pi = \Pi_f \circ \Pi_h \circ \Pi_f \circ \Pi_l : I_l \rightarrow I_l. \tag{15}$$

This construction shows that the stable manifold of x_m divides the state space into two invariant sets. One is the basin of attraction of x_l , while the other one has dynamics characterized by the Poincaré map (15). Since this is a smooth map of an interval into itself it admits at least one fixed point, which corresponds to a singular relaxation oscillation. As shown in [14], if this fixed point is hyperbolic, under the additional hypothesis that the singular trajectory intersects P_l and P_h transversally, it perturbs to a hyperbolic limit cycle for $\varepsilon > 0$. In fact the Poincaré map (15) is (up to conjugacy) a global version of the one used in that reference.

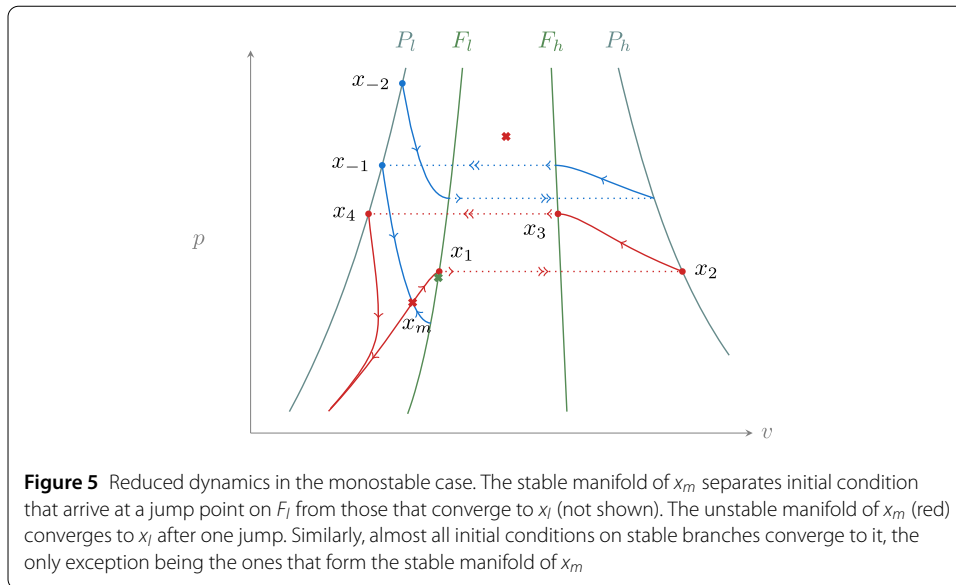
We remark that this construction only guarantees multistability. Further analysis of the map (15) is required to obtain a more accurate picture. While this is beyond the scope of this work, numerical simulations confirm that this map has a unique attracting fixed point.

4.2 Monostability

Constructing the Poincaré map (15) requires that x_4 falls inside the interval defined by x_{-1} and $p = g_p$ on P_l . The situation in which this assumption fails is illustrated in Fig. 5. In this case most trajectories on S_l and S_h are attracted by the stable fixed point x_l , the only exception being the stable manifold of x_m .

To see this, we start from x_{-1} and consider its anti-image through Π_f on F_h . Continuing to follow the singular flow “backwards”, as shown in Fig. 5, leads back to P_l at a point that we call x_{-2} . Any compact segment in P_l that lies between these points is mapped by the singular flow strictly inside the segment delimited by x_4 and x_{-1} . Since any point strictly inside this second segment converges to x_l , the same conclusion extends to all points in the original segment.

The same argument shows that points in the portion of S_l delimited by the trajectories starting at x_{-1} and x_{-2} tend to x_l . The only exceptions are these boundary trajectories that reach x_m and belong to its stable manifold. As long as the stable manifold of x_m is unbounded in the p coordinate, the same argument can be iterated on all S_l and adapted to S_h , leading to the conclusion that almost all points on S_l and S_h are in the basin of attraction of x_l . This situation persists for small enough $\varepsilon > 0$, and since most points are attracted to stable branches of the slow manifold we see that for almost all initial conditions the perturbed dynamics converges to x_l .



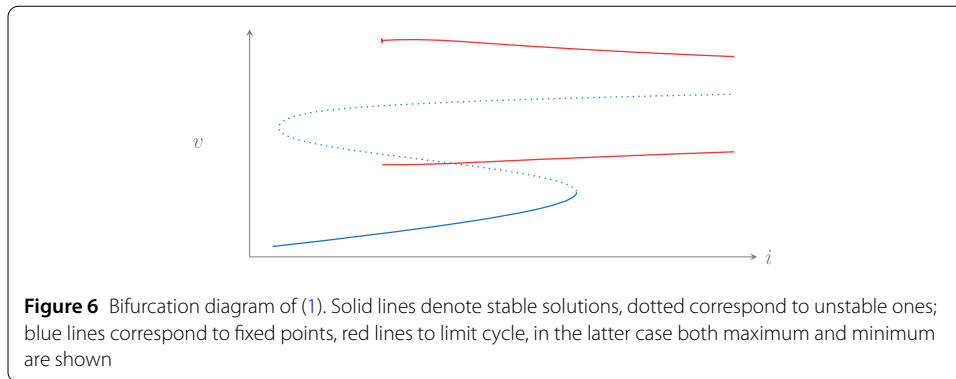
4.3 Homoclinic trajectory and bifurcation diagram

Transitions between monostability and bistability in system (1) are controlled by the applied current i . The phase portraits in Figs. 4 and 5 suggest the presence of a homoclinic trajectory, which can be obtained by decreasing the applied current from the bistable case. In the singular limit this trajectory corresponds to the condition $x_4 = x_{-1}$ and delimits the boundary of bistability. We denote by i_H the value of current at which this happens. While we cannot expect this homoclinic trajectory to persist for $\varepsilon > 0$ with i fixed, it is natural to ask whether for $\varepsilon > 0$, fixed and small, we can find an $i_H(\varepsilon)$, close to i_H , at which a homoclinic trajectory exists. There is a natural transversality condition that guarantees this property. The family of fixed points $x_m(i)$ admits a three-dimensional stable manifold and a two-dimensional unstable one. Their intersection is a homoclinic trajectory. In the singular limit, following the unstable manifold of $x_m(i)$ leads back to S_l after two jumps. Extending \mathcal{C}_0 to include i , $x_m(i)$ is a (normally hyperbolic) invariant set in it, with two-dimensional invariant manifolds. The continuation of the unstable one using the singular flow, after two jumps intersects the stable manifold in the plane $i = i_H$. If this intersection is transverse then it persists for small ε and i close to i_H . We show this in Appendix A adapting the arguments used in [14] to prove existence of relaxation oscillations.

To conclude this section, Fig. 6 shows the bifurcation diagram of the whole system (1) computed with AUTO-07p [18] for parameter values reported in Appendix B. The numerics confirms the presence of a family of limit cycle (red curves) and its coexistence with a family of fixed points (blue curve). The family of periodic solutions terminates in a homoclinic trajectory for low values of i (the numerical continuation was stopped at period $T = 10^4$).

5 A common geometric picture

The bifurcation diagram illustrated in the previous section is understandably only one among many possible scenarios compatible with the three-dimensional geometry of Fig. 2. While a detailed study of all possible cases is beyond the scope of this work, we wish to highlight how different types of bistability could have the same geometric structure. To do



this we use ideas and techniques from [19]. As in Sect. 3 we identify fixed points with the $i-v$ curve

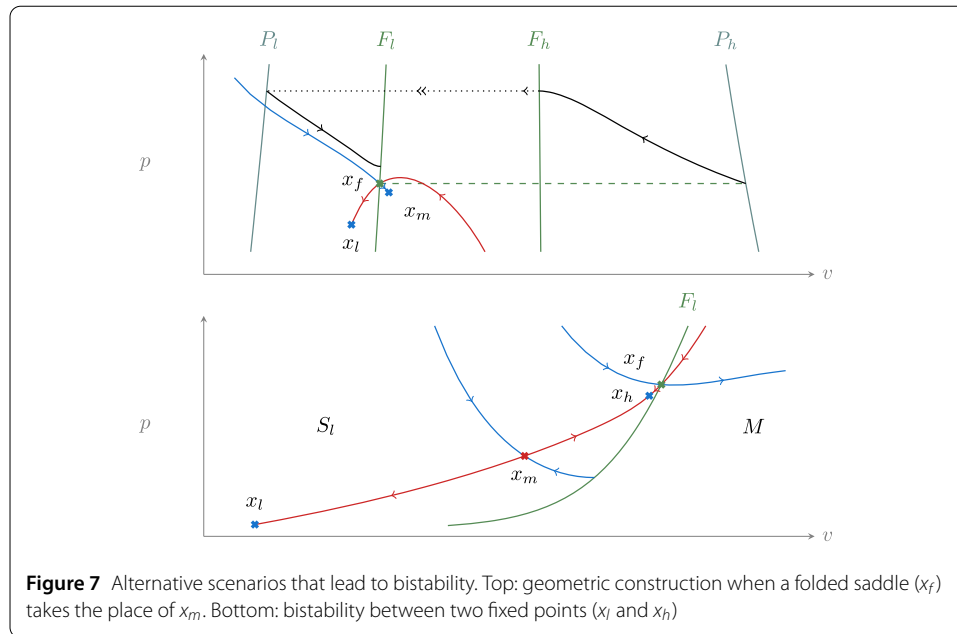
$$i_s(v) = i_{\text{ion}}(v, S_n(v), S_p(v)) \tag{16}$$

and divide them in three families $\mathcal{X}_l, \mathcal{X}_m$ and \mathcal{X}_h , separated by two folds. As noted in Sect. 3 there is a value of current i_c , between the two folds, at which x_m crosses F_l to enter the unstable branch M . The scenario studied in Sect. 4 assumes $i_c < i_H$ since the homoclinic bifurcation occurs when $x_m \in S_l$.

As a first variation we consider what happens when the bistable range extends to current values for which $x_m \in M$. The bifurcation $x_m \in F_l$ corresponds to a folded saddle-node. Beyond this bifurcation $x_m \in M$ is a node of the reduced dynamics while x_f is a saddle. In this case the analysis is easily adapted from Sect. 4. One must simply substitute the stable manifold of x_m with the one of x_f , and use $\Pi_f(x_f)$ in place of $x_2 = \Pi_f(x_1)$. Figure 7 shows the corresponding geometric construction. A classical example where this scenario occurs is the Hodgkin–Huxley model with the reversal potential of potassium increased. This situation of bistability has been studied in the early work [20]. Its planar reduction leads to the transcritical model [10]. Also in this case the boundary of bistability is a singular homoclinic trajectory. This trajectory, however, has to go through the folded singularity x_f to reach x_m on the unstable branch M .

Both cases discussed so far assume that x_m and x_h collide in a fold on M . Yet another scenario corresponds to this fold occurring on S_l , after x_h crosses F_l . Also this crossing leads to a folded saddle-node, after which $x_h \in S_l$ can perturb to a stable fixed point. Local analysis around folded saddle-node shows the possibility of Hopf bifurcations [17], which are indeed found numerically. After this the system presents two stable fixed points. The relevant part of the reduced dynamics in this case is shown in Fig. 7: the stable manifold of x_m acts as separatrix between the basins of attraction of the two stable fixed points, while the one of x_f (a folded saddle) separates initial conditions that reach a jump point on F_l from those that remain on the critical manifold.

The examples above suggest that many possible variants for transitions between monostability and bistability are possible. We also note that many of the geometric constructions used in [6, 7, 19] have an analog in our setting, allowing, for example, non-plateau oscillations, contrary to the case showed in Fig. 1. This flexibility is interesting in the perspective of connecting the present approach to the classification of bursting types according to the transitions that occur from rest to spike and vice versa (see e.g. [21]).

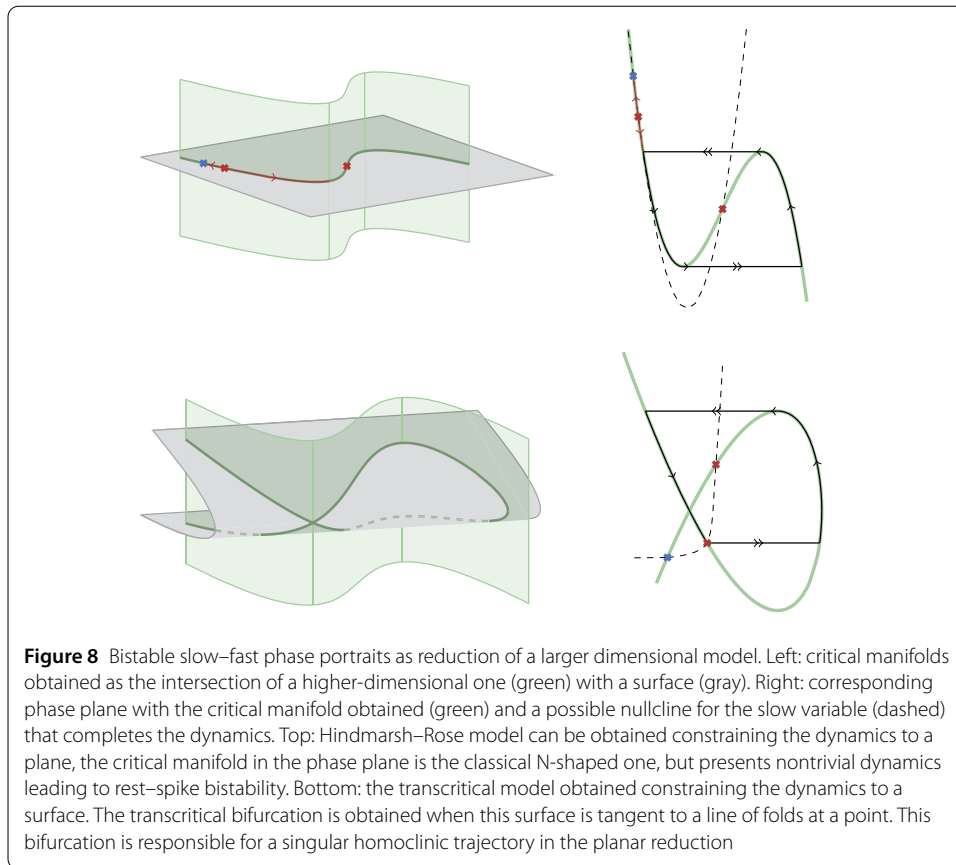


6 Connections with phase-portrait analysis

We close this paper by clarifying the connection between the proposed three-dimensional model and two published slow–fast phase portraits of rest–spike bistability.

The first phase portrait goes back to the seminal work of Hindmarsh and Rose [8, 22]. In one of the earliest attempts to model slow spiking and bursting, Hindmarsh and Rose proposed to modify the FitzHugh–Nagumo model with a recovery variable that has a nonmonotonic activation function. Geometrically, this situation corresponds to a degenerate case of the planar pictures described in Sect. 3 and Sect. 4, in which all essential elements are contained on a line. As a result, the main elements of the three dimensional dynamics can be captured by constraining it to a plane, resulting in a simplified two-dimensional model of rest–spike bistability. This is characterized by the classical N-shaped critical manifold, as shown in Fig. 8. The price paid for this simplification is that the flexibility of the two-dimensional slow dynamics described in Sect. 5 is lost. For instance, bistability is only possible if x_l lies out of the stripe delimited by P_l and F_l , ruling out patterns in which the voltage of the resting state is between maximum and minimum of the spike. We note that the nonmonotonicity of the activation function in Hindmarsh–Rose model has the natural interpretation of summarising in one variable the distinct roles of an inward and an outward slow current.

The second rest–spike bistable phase portrait is the transcritical model of [6]. This model was obtained as a two-dimensional reduction of a conductance-based model that adds a slow calcium current to the Hodgkin–Huxley model [9]. The analysis of [6] rests on the presence of a transcritical bifurcation of the critical manifold. This bifurcation also directly relates to the mixed role of the slow variable as a source of both positive and negative feedback in the slow time-scale. A main motivation of the present paper was to understand the geometric picture generated by this motif in conductance-base models, where these two roles are often played by distinct variables.



To connect the transcritical bifurcation of the planar model [6] to the three-dimensional geometry of the present paper we consider how this planar reduction can be obtained. Referring to our model (1) for simplicity, a planar reduction is typically obtained imposing an algebraic constraint between n and p , which can be interpreted as a path $n(s), p(s)$ [20]. After obtaining a dynamic equation for s from a combination of \dot{n} and \dot{p} , the system becomes

$$\begin{aligned} \varepsilon \dot{v} &= i - i_{\text{ion}}(v, n(s), p(s)), \\ \dot{s} &= g(v, s), \end{aligned} \tag{17}$$

which is a slow-fast planar model. Its critical manifold is given by

$$i = i_{\text{ion}}(v, n(s), p(s)) \tag{18}$$

It corresponds to the intersection of the critical manifold of the larger system with the surface

$$n = n(s), \quad p = p(s). \tag{19}$$

A transcritical bifurcation is obtained when

$$\begin{aligned}
 & i_{\text{ion}} = i, \\
 & \frac{\partial i_{\text{ion}}}{\partial v} = 0, \\
 & \frac{\partial}{\partial s} (i_{\text{ion}}(v, n(s), p(s))) = \frac{\partial i_{\text{ion}}}{\partial n} \frac{dn}{ds} + \frac{\partial i_{\text{ion}}}{\partial p} \frac{dp}{ds} = 0.
 \end{aligned}
 \tag{20}$$

Geometrically this corresponds to a point at which the surface (19) is tangent to the line of folds of the critical manifold, as shown in Fig. 8. Similar geometric constructions lead to the presence of a transcritical bifurcation when reducing the Hodgkin–Huxley model with increased potassium reversal potential, as well as when reducing the same model augmented with a calcium current, as done in [6].

An equivalent interpretation of how the transcritical bifurcation arises is that the path $(n(s), p(s))$ defining the surface (19) is tangent to the line of folds

$$i = i_{\text{ion}}(v, n, p), \quad \frac{\partial i_{\text{ion}}}{\partial v}(v, n, p) = 0,
 \tag{21}$$

projected onto the n – p plane. This is the simplest example of how singularities in the sense of [23] can be generated from elementary catastrophes, the core idea in the path formulation of [23, Ch.3 §12]. This is particularly interesting in view of [24], where singularity theory is used to obtain a global description of the critical manifolds of slow–fast planar systems relevant to neuronal dynamics. Two singularities play a prominent role: hysteresis, in connection with spiking, and winged cusp, for rest–spike bistability. Both these singularities can be realized as paths in the unfolding of the cusp catastrophe [23]. Interestingly, this bifurcation is often found in the fast subsystem of neuronal models (an early example being [25]), and it is typically related to the appearance and disappearance of bistability. For example, decreasing the sodium conductance in the Hodgkin–Huxley model leads to the appearance of this bifurcation, and the same is achieved by reducing g_m in (1). The presence of this type of bifurcation in these models suggests that those singularities can arise from model reduction similarly to what happens in the transcritical case.

7 Conclusions

We studied a simplified slow–fast model of neuronal activity that exhibits rest–spike bistability. The simplest physiological models of excitability include a fast-activating inward current and a slowly-activating outward current. Our model adds a slowly-activating inward current to this basic motif. We think of this model as a core structure for the generation of multistability in more general and realistic conductance-based models. We speculate that similar results are possible using a slowly inactivating outward current, which would have the same functional role of a slow positive feedback.

Through geometric singular perturbation theory we could analyze the geometry of this three-dimensional model. This geometry is rather simple, with the slow dynamics taking place on a classical N-shaped critical manifold. The saddle point on the critical manifold is a key feature of the proposed model. Its stable manifold acts as separatrix, while its unstable manifold determines whether multiple attractors are present. Moreover, a same

geometric picture captures different types of bistability, suggesting a common framework to study different phenomena important to neuronal dynamics.

This is by no means the first study of a slow–fast systems with one fast and two slow variables, nor the first single-cell model of bistability. The value of this model is in that it explains how bistability can arise in a physiologically relevant context using a mechanism that is generic but not widely acknowledged. Our hope is that it contributes to the view that a combination of positive and negative feedback in the slow time-scale is a core element in the generation of neuronal patterns.

Appendix A: Existence of a homoclinic trajectory

In this section we show that under the assumption of transversality, the intersection of stable and unstable manifolds that leads to a singular homoclinic trajectory persists for $\varepsilon > 0$. We do this using the setting of [14] and in particular their results on maps defined by the flow of (1). We recast these results in the notation of Sect. 4 and refer the reader to the original work for details.

As in Sect. 4, i_H is the value of i at which a singular homoclinic trajectory exists. We consider the reduced dynamics for this value of i , and fix a point x_u on the unstable manifold of x_m between x_m and F_l . Similarly, we fix a point x_s on the stable manifold between P_l and x_m .

After a local change of coordinates we can find two neighborhoods of these points, N_s and N_u , such that the critical manifold \mathcal{C}_0 corresponds to the plane $v = 0$. The intersections of these neighborhoods with the planes $n = n_s$ and $n = n_u$ determine two surfaces Σ_s and Σ_u . Rotating n and p if necessary, we can assume that $\Sigma_u \cap \mathcal{C}_0$ intersects the unstable manifold of x_m transversally and only at x_u , and similarly for $\Sigma_s \cap \mathcal{C}_0$. For fixed δ we let $N_\delta = (i_H - \delta, i_H + \delta)$ and consider $\Sigma_s \times N_\delta$ and $\Sigma_u \times N_\delta$. If δ is small enough, stable and unstable manifolds of $x_m(i)$ intersect transversally these extended neighborhoods (in the critical manifold extended to include i). In the following we assume that N_s, N_u, N_δ are shrunk whenever necessary.

In Sect. 3, we have characterized the stable manifold of x_m for small $\varepsilon > 0$, this is composed of a line on \mathcal{C}_ε and the fibers based on it. In the limit $\varepsilon \rightarrow 0$, the singular stable manifold intersect Σ_s transversally along one of these fibers. Thus if ε and δ are small enough the same will be true for the stable manifold of $x_m(i)$ for fixed i and ε . Moreover, since at $\varepsilon = 0, i = i_H$ this intersection is a line of constant p , we can find a parametrization of it that has the form $p = p_s(v, i, \varepsilon)$. Similarly, the intersection of Σ_u with the unstable manifold of $x_m(i, \varepsilon)$ defines two functions $v_u(i, \varepsilon)$ and $p_u(i, \varepsilon)$.

Notice that in this section we use v and p to parametrize the two slices Σ_s and Σ_u , so that v preserves its nature of fast variable. This differs from the use of v and p to parametrize the critical manifold as done in Sect. 3 and Sect. 4.

We can now use the same construction of [14] to obtain a map $\Pi : \Sigma_u \rightarrow \Sigma_s$ corresponding to the action of the flow. This has the form

$$\Pi \begin{pmatrix} v \\ p \end{pmatrix} = \begin{pmatrix} R(v, p, i, \varepsilon) \\ G(v, p, i, \varepsilon) \end{pmatrix}; \tag{22}$$

R is exponentially small in ε ($|R| + \|\nabla R\| < \exp(-c/\varepsilon)$) and in particular verifies

$$R(v, p, i, 0) = 0. \tag{23}$$

G has the form

$$G = G_0(p) + \mathcal{O}(\varepsilon \ln(\varepsilon)) \tag{24}$$

where $G_0 : \Sigma_u \cap \mathcal{C}_0 \rightarrow \Sigma_s \cap \mathcal{C}_0$ is the map defined by the singular flow. Smooth dependence on i follows from standard results.

The only difference between this map and the Poincaré map defined in [14] is that we consider two different sections Σ_s and Σ_u rather than one.

Applying this map to (v_u, p_u) we obtain the intersection of the unstable manifold of x_m with Σ_s

$$\Pi \begin{pmatrix} v_u \\ p_u \end{pmatrix} = \begin{pmatrix} R(v_u, p_u, i, \varepsilon) \\ G(v_u, p_u, i, \varepsilon) \end{pmatrix}. \tag{25}$$

In this setting an intersection of stable and unstable manifolds corresponds to a solutions of

$$G(v_u, p_u, i, \varepsilon) = p_s(R(v_u, p_u, i, \varepsilon), i, \varepsilon) \tag{26}$$

where $v_u = v_u(i, \varepsilon)$ and $p_u = p_u(i, \varepsilon)$. Thus, we can define

$$P_u(i, \varepsilon) = G(v_u, p_u, i, \varepsilon), \quad P_s(i, \varepsilon) = p_s(R(v_u, p_u, i, \varepsilon), i, \varepsilon) \tag{27}$$

and a homoclinic trajectory corresponds to $P_u - P_s = 0$.

At $\varepsilon = 0$

$$\begin{aligned} P_u(i, 0) &= G_0(p_u(i, 0)), \\ P_s(i, 0) &= p_s(R(0, p_u(i, 0), i, 0), i, 0) = p_s(0, i, 0), \end{aligned} \tag{28}$$

and the existence of the singular homoclinic trajectory at $i = i_H$ means that

$$P_u(i_H, 0) = G_0(p_u(i_H, 0)) = p_s(0, i_H, 0) = P_s(i_H, 0). \tag{29}$$

Assuming that

$$\frac{\partial P_u}{\partial i}(i_H, 0) - \frac{\partial P_s}{\partial i}(i_H, 0) \neq 0, \tag{30}$$

an application of the implicit function theorem^b guarantees the existence of a continuous functions $i_H(\varepsilon)$ such that $P_u(i_H(\varepsilon), \varepsilon) = P_s(i_H(\varepsilon), \varepsilon)$.

At $\varepsilon = 0$, $P_u(i, 0)$ is the intersection of the singular unstable manifold (after two jumps) with $\Sigma_s \cap \mathcal{C}_0$, while $P_s(i, 0)$ corresponds to the intersection of the stable manifold of the reduced flow and $\Sigma_s \cap \mathcal{C}_0$. Condition (30) corresponds to transversality of the intersection between the manifolds $p = P_s(i, 0)$ and $p = P_u(i, 0)$ in the extended neighborhood $\Sigma_s \times N_\delta$. Since the invariant manifolds of $x_m(i)$ can be obtained applying the singular flow to these two sections, we see that condition (30) is equivalent to transversality of the intersection between the invariant manifolds of $x_m(i)$ on the critical manifold (where the unstable manifold has been continued past two jumps using the singular flow).

Appendix B: Parameters

The analysis in Sects. 3 and 4 uses the following numerical values for the parameters of (1)

$$\begin{aligned}\varepsilon &= 0.05, & v_l &= -0.8, & gl &= 2, \\ g_m &= 4.4, & a_m &= -0.19, & b_m &= 0.18, \\ g_n &= 8.0, & a_n &= -0.16, & b_n &= 0.29, \\ g_p &= 2.0, & a_p &= -0.5, & b_p &= 0.3, \\ \tau &= 1.5.\end{aligned}\tag{31}$$

Acknowledgements

Not applicable.

Funding

GIC has received funding from EPSRC (RG80792) and Qualcomm Inc. The research leading to these results has received funding from the European Research Council under the Advanced ERC Grant Agreement Switchlet n.670645.

Abbreviations

Not applicable.

Availability of data and materials

Not applicable.

Ethics approval and consent to participate

Not applicable.

Competing interests

The authors declare that they have no competing interests.

Consent for publication

Not applicable.

Authors' contributions

All authors formulated the problems. GIC carried out the details of the theoretical analysis and performed the simulations. All authors wrote, read and approved the manuscript.

Endnotes

^a This assumes that the bifurcation does not happen exactly on F_j .

^b We need a relaxed version of the implicit function theorem since the dependence on ε is not smooth but only continuous; this is proven in [26].

Publisher's Note

Springer Nature remains neutral with regard to jurisdictional claims in published maps and institutional affiliations.

Received: 7 February 2020 Accepted: 25 August 2020 Published online: 04 September 2020

References

1. Hodgkin AL, Huxley AF. A quantitative description of membrane current and its application to conduction and excitation in nerve. *J Physiol.* 1952;117(4):500–44.
2. Morris C, Lecar H. Voltage oscillations in the barnacle giant muscle fiber. *Biophys J.* 1981;35(1):193–213.
3. FitzHugh R. Impulses and physiological states in theoretical models of nerve membrane. *Biophys J.* 1961;1(6):445–66.
4. Ermentrout GB, Terman DH. *Mathematical foundations of neuroscience.* New York: Springer; 2010.
5. Izhikevich EM. *Dynamical systems in neuroscience.* Cambridge: MIT Press; 2006.
6. Franci A, Drion G, Sepulchre R. An organizing center in a planar model of neuronal excitability. *SIAM J Appl Dyn Syst.* 2012;11(4):1698–722.
7. Franci A, Drion G, Sepulchre R. Robust and tunable bursting requires slow positive feedback. *J Neurophysiol.* 2018;119(3):1222–34.
8. Hindmarsh JL, Rose RM. A model of the nerve impulse using two first-order differential equations. *Nature.* 1982;296(5853):162–4.
9. Drion G, Franci A, Seutin V, Sepulchre R. A novel phase portrait for neuronal excitability. *PLoS ONE.* 2012;7(8):e41806.

10. Franci A, Drion G, Seutin V, Sepulchre R. A balance equation determines a switch in neuronal excitability. *PLoS Comput Biol*. 2013;9(5):e1003040.
11. Drion G, O'Leary T, Marder E. Ion channel degeneracy enables robust and tunable neuronal firing rates. *Proc Natl Acad Sci USA*. 2015;112(38):E5361–70.
12. Fenichel N. Geometric singular perturbation theory for ordinary differential equations. *J Differ Equ*. 1979;31(1):53–98.
13. Szmolyan P, Wechselberger M. Canards in \mathbb{R}^3 . *J Differ Equ*. 2001;177(2):419–53.
14. Szmolyan P, Wechselberger M. Relaxation oscillations in \mathbb{R}^3 . *J Differ Equ*. 2004;200(1):69–104.
15. Wechselberger M, Mitry J, Canard RJ. Theory and excitability. In: *Lecture notes in mathematics*. Berlin: Springer; 2013. p. 89–132.
16. Szmolyan P. Transversal heteroclinic and homoclinic orbits in singular perturbation problems. *J Differ Equ*. 1991;92(2):252–81.
17. Krupa M, Wechselberger M. Local analysis near a folded saddle-node singularity. *J Differ Equ*. 2010;248(12):2841–88.
18. Doedel EJ, Fairgrieve TF, Sandstede B, Champneys AR, Kuznetsov YA, Wang X. AUTO-07P: continuation and bifurcation software for ordinary differential equations. 2007.
19. Ribar L, Sepulchre R. Neuromodulation of neuromorphic circuits. *IEEE Trans Circuits Syst I, Regul Pap*. 2019;66(8):3028–40.
20. Rinzel J. Excitation dynamics: insights from simplified membrane models. In: *Fed. proc. vol. 44*. 1985. p. 2944–6.
21. Izhikevich EM. Neural excitability, spiking and bursting. *Int J Bifurc Chaos*. 2000;10(6):1171–266.
22. Hindmarsh JL, Rose RM. A model of neuronal bursting using three coupled first order differential equations. *Proc R Soc Lond B, Biol Sci*. 1984;221(1222):87–102.
23. Golubitsky M, Schaeffer DG. *Singularities and groups in bifurcation theory*. New York: Springer; 1985.
24. Franci A, Drion G, Sepulchre R. Modeling the modulation of neuronal bursting: a singularity theory approach. *SIAM J Appl Dyn Syst*. 2014;13(2):798–829.
25. Zeeman EC. Differential equations for the heartbeat and nerve impulse. In: *Dynamical systems*. Amsterdam: Elsevier; 1973. p. 683–741.
26. Loomis LH, Sternberg S. *Advanced calculus*. Singapore: World Scientific; 2013.

Submit your manuscript to a SpringerOpen[®] journal and benefit from:

- Convenient online submission
- Rigorous peer review
- Open access: articles freely available online
- High visibility within the field
- Retaining the copyright to your article

Submit your next manuscript at ► [springeropen.com](https://www.springeropen.com)
